Chemical composition and oxidative potential of atmospheric coarse particles at an industrial and urban background site in the alpine region of northern Italy

Maria Chiara Pietrogrande[1], Cristina Dalpiaz[2], Rossana Dell'Anna[3], Paolo Lazzeri[2], Francesco Manarini[1], Marco Visentin[1], Gabriele Tonidandel[2]

[1]Department of Chemical and Pharmaceutical Sciences, University of Ferrara, Via Fossato di Mortara 17/19 - 44121 Ferrara, Italy.

[2] Agenzia Provinciale Protezione Ambiente, via Lidorno 1 - 38123 Trento, Italy

[3] Fondazione Bruno Kessler, Centre for Materials and Microsystems, Micro Nano Facility, Via Sommarive 18, 38123 Trento, Italy.

Corresponding author: Prof. M.C. Pietrogrande, email: mpc@unife

Abstract

Particulate matter (PM) PM_{10} samples were collected at industrial (Ala) and background (TN) sites in the alpine region of northern Italy with the aim to investigate the possible impacts of emissions from the industrial site on chemical composition and on the oxidative potential on airborne particulate Detailed chemical analyses were performed to characterize the chemical composition of the collected samples, likely to identify specific chemical components characterizing the emissions sources impacting the area. Source apportionment study based on Positive Matrix Factorization identified that the main emission sources of airborne metals at Ala are a zinc coating facility located in the area, traffic on a congested motorway and pesticide/fungicide normally used in the vineyard district an area.

Redox activity of the PM_{10} samples was measured by means of two a-cellular assays, i.e., dithiothreitol (DTT) and ascorbic acid (AA) assays.

The responses of the DTT assay (volume-normalized OP^{V}_{DTT}) are similar at both sites (mean values: 0.60±0.23 mmol min^{-1} m^{-3}) while those of the AA assay (volume-normalized OP^{V}_{AA}) show significantly higher values at Ala (1.4±1.1 nmol min^{-1} m^{-3}) than at TN (0.7±0.4 nmol min^{-1} m^{-3}). This is consistent with the different sensitivity of the two assays towards the same redox-active species present in ambient PM, as elucidated by linear correlation analysis of OP^{V} with the concentration of tracer pollutants and highlighted by Heat Maps representation. At the industry site OP^{V}_{DTT} is correlated only with potassium and rubidium (R ~ 0.8), while OP^{V}_{AA} almost exclusively with Cu (R= 0.88). Otherwise, at TN both OP^{V}_{DTT} and OP^{V}_{AA} are both correlated with several species ($R \geq 0.7$), such as WSTC, SO_4^{2-}, NH_4^{+}, K, Mn, Cu and Zn. In addition, at Ala pronounced day-of-week evolution was observed for OP^{AA}_{V} values confirming the contribution of heavy metals from the anthropogenic sources.

Key words

Coarse particles PM_{10},
Oxidative potential,
Industrial emissions,
Source apportionment.

Introduction

Air pollution continues to receive a great deal of interest worldwide due to its negative impacts on human health, including cardiovascular diseases, respiratory problems, and adverse neurodevelopmental effects (Davidson et al., 2005; Jansen et al., 2005; Brook et al., 2010; Chen et al., 2013). As ambient particles consist of a wide range of chemical components of potentially varying toxicity, a proper air quality metric for assessing health impacts has to be based overall on

the recognition of the pollution sources and on the assessment of their contribution on PM (Li et al., 2008; Val et al., 2011; Pietrogrande et al., 2015; Shuster-Meiseles et al., 2016). Among the sources of air pollution traffic (mobile sources), combustion processes and industrial activities (fixed sources) have been found to have likely the largest effects, as they produce and continuously emit into the atmosphere gaseous, black carbon (or elemental carbon and associated species) (Jansen et al., 2005), polycyclic aromatic hydrocarbons (PAHs) (Akhtar et al., 2010; Jansen et al., 2014; Bates, et al., 2015).

Although a comprehensive set of mechanisms explaining the observed linkage between PM mass and adverse health effects has not been established, there is increasing evidence that oxidative stress may be one of the unifying mechanisms underlying toxicity of exposure to airborne particles. It ensues when ROS production exceeds the cell's ability to scavenge and inactivate oxygen radicals. Atmospheric particles have been shown to generate reactive oxygen species (ROS, i.e., H_2O_2 and free radicals such as the hydroxyl radicals and superoxide ions, that can induce oxidative stress in pulmonary systems, followed by a cascade of inflammation responses, including activation of various transcription factors and stimulation of cytokine production (Akhtar et al., 2010; Chung et al., 2006; Peters et al., 2006; Li et al., 2008; Bates et al., 2015; Verma et al., 2015; Antiñolo et al., 2015). Consistently with the above notion, the ability of PM to generate ROS in the respiratory tract was suggested as a proper metric that could provide insights into the toxicological responses to atmospheric aerosol exposure. Thus, the oxidative potential (OP) is defined as a measure of the capacity of PM to oxidise target molecules to generate ROS and the resulting oxidative stress (Li et al., 2002; Ayres et al., 2008; Li et al., 2008; Saffari et al., 2014; Hedayat et al., 2014; Crobeddu et al., 2017).

The aim of the present investigation is to assess the possible impact of airborne metals on air quality and on oxidative potential of PM_{10} and likely to identify any association with specific chemical components characterizing the emissions sources impacting an area hosting a zinc coating industry.

With this in mind, two intensive air monitoring campaigns were performed in a local area, the Adige valley, in the alpine region of northern Italy, at an industrial (Ala) and at a neighbouring urban background site (Trento, TN). The Ala site (45.8 N, 11.0 E) hosts a zinc coating facility adopting hot dip technology. Ala is also close to the traffic congested A-22 Brenner motorway, the main route connecting Italy to Austria and northern Europe, and is impacted by emissions due to wood burning for domestic heating during the cold seasons, as commonly found in other sites in the alpine area (Sandrini et al., 2014, Perrino et al., 2014, Herich, et al., 2014; Pietrogrande et al., 2015; APPA Trento, unpublished data). Additionally, pesticide/fungicide spraying in intensive vineyard cultivation in the district is likely a further source of aerosol pollution. The urban background site of Trento (46.0 N, 11.1 E) is located about 40 km north from Ala. This location was selected to highlight, at the best possible way, the direct impact of local sources of pollution, including the fugitive dust possibly related with the zinc coating industry, over the contribution of non-local PM sources (regional background) that were argued to impact uniformly in the two sites.

The chemical composition of the collected filters was characterized and a source apportionment study was conducted in order to identify the main sources of aerosol.

The oxidative potential was measured by means of two common a-cellular assays, among several a-cellular assays developed to quantify the oxidative potential of PM samples, i.e., dithiothreitol, (DTT) and ascorbic acid (AA) assays. They are simple cell-free procedures that measure the capacity of PM extracts to oxidize target antioxidants simulating the PM−cell interaction leading to the generation of ROS. The DTT assay uses DTT as a chemical surrogate of cellular antioxidants, such as glutathione and NADPH (nicotinamide adenine dinucleotide phosphate) (Cho et al., 2005; Charrier and Anastasio, 2012; Hedayat et al., 2014; Janssen et al., 2014; Verma et al., 2015; Charrier et al., 2015; Fang et al., 2016; Antiñolo et al., 2015). The ascorbic acid assay is based on AA, that is a physiological antioxidant in the respiratory tract lining fluids (RTLFs), which prevents the oxidation of lipids and proteins (Mudway et al., 2004; Ayres et al., 2008; DiStefano et al., 2009; Fang et al., 2016).

103103

104 Material and methods

105105

106 Sampling sites and periods

107 A first sampling campaign was conducted from early spring and later on in summer-autumn by
108 collecting nearly 160 PM_{10} samples (from February 25th to November 07th 2015, except a part of
109 May and June). The second sampling period was intentionally selected during the warmer months
110 of the year to minimize the contribution of biomass burning to PM mass. Thus, 21 PM_{10} samples
111 were collected from April 8th to May 9th. During both sampling campaigns, the Zn coating facility
112 was regularly in operation. During both sampling campaigns parallel PM10 samples were collected
113 at the industrial Ala and urban background (TV) sites.

114114

115 Sampling and chemical analyses

116 Daily PM_{10} samples were collected by using low-volume sequential samplers (TCR-Tecora
117 Skypost) operating at a flow rate of 38 L min^{-1} corresponding to an air volume of about 55 m^3 per
118 day. Teflon membranes (Pall Teflo) were used for the source apportionment study (1st campaign),
119 whilst quartz filters (Pall Tissuquartz QAO-UP, pre-baked in muffle at 550 °C) for oxidative
120 potential measurements (2nd campaign). The samples were stored at 4°C until chemical analyses
121 were undertaken.
122 The samples collected on teflon membranes were submitted to Energy Dispersive X-Ray
123 Fluorescence analysis (Panalytical Epsilon 5) to determine elemental composition. Subsequently,
124 they were extracted with water to measure anions and oxalate, cations and sugars.
125 Samples collected on quartz filters were analysed only for the water soluble fraction, as it better
126 represents the bioavailable part on which the oxidative potential is measured. Soluble trace metals
127 were also measured in this case, along with water soluble total carbon (WSTC). Sample aliquots
128 were extracted by sonication with 5 ml of ultra-pure water for 30 min filtered with 0.45 μm Pall

Acrodisk membranes and submitted to analysis of 26 individual chemical components. Anions (including oxalate) and cations were determined by Ion Chromatography (Dionex ICS-2500 and Dionex DX-600) by using Dionex AS11-HC and CS16 analytical columns with soda and methanesulfonic acid as eluents, respectively. Anidrosugars, with biogenic markers polyols and glucose were determined by High Performance Anion Exchange Chromatography-Pulsed Amperometry Detection, with a Dionex ICS-2500 amperometric cell equipped with Au disposable electrode, Metrohm Metrosep Carb 2 column and soda as eluent. Trace elements were determined by ICP-MS (Agilent Technology 7700) after acidification with ultrapure nitric acid. WSTC was determined by a Total Carbon Analyser (Shimadzu TOC 5000A).

138138

Toxicological analyses: measurements of Oxidative Potential

Oxidative potential of the PM samples was quantified using the Dithiothreitol and Ascorbic Acid assays described elsewhere (Visentin et al., 2016). Both assays were performed under operative conditions mimicking in vivo interactions with cellular antioxidants, i.e. 37°C and pH 7.4.

Briefly, in the DTT assay 30 µl of the DTT 10 mM solution were added to the sample. At known times, a 0.50 mL aliquot of the reaction mixture was removed and added to 0.50 mL of 10 % trichloroacetic acid to stop the reaction. When all time points were quenched, 50 µL of 10.0 mM DTNB (5,5'-Dithiobis(2-nitrobenzoic acid)) (made in 10.0 mM phosphate buffer at pH 7.4) were added, well mixed, and allowed to react for 2 minutes, then 2.0 mL of 0.40 M Tris-Base (pH 8.9) were added. The reaction of DTT and DTNB forms 2-nitro-5-thiobenzoic acid (TNB), that was quantified by measuring UV absorbance at 412 nm (ε =14150 M^{-1} cm^{-1}) (Charrier and Anastasio, 2012; Fang et al., 2016).

In the AA assay 30 µl of the AA solution 10 mM were added to the sample and the absorbance of the ascorbate ion AA directly measured in the spectrophotometric cuvette at 265 nm (ε =14500 $M^{-1}cm^{-1}$) (Mudway et al., 2004; Ayres et al., 2008).

Spectrophotometric measurements were performed in a UV-Vis spectrophotometer (Varian Cary 50) with a 1 cm path length optical cell. Polystyrene and quartz cuvette were used for DTT and AA assays, respectively.

OP of ambient PM was assessed by performing each assay on 3 mL of the aqueous solution obtained by extracting a quarter of the sampled filters with 10 mL of 0.1 M phosphate buffer (pH 7.4) for 15 minutes in an ultrasonic bath.

The rate of DTT or AA depletion (nmol min^{-1}) was determined by linear fitting the experimental points of the reagents concentration versus time (5, 10, 15, 25, 40 minutes) (Visentin et al., 2016). The response of blank filters were determined and subtracted from the data of real PM samples. These values were normalized by the volume of sampled air (OP^{V}_{DTT} and OP^{V}_{AA} expressed as nmol min^{-1} m^{-3}) to represent the effective human exposure to PM_{10} in the inhaled air. In addition, OP_{DTT} and OP_{AA} were related by the PM_{10} mass (OP^{m}_{DTT} and OP^{m}_{AA} expressed as nmol min^{-1} μg^{-1}) to point out the intrinsic ability of the particles to deplete physically relevant antioxidants.

167167

Positive Matrix Factorization technique

Source apportionment was assessed using Positive Matrix Factorization (PMF), a widely-used receptor model initially developed by Paatero and Tapper (1994), where concentration values are weighed taking into account the analytical uncertainty of measured concentrations, missing data, values below the minimum detection limit as well as outliers. In this work, the program EPA PMF 5.0 was used, following the recommendations described in Belis, et al. (2014, and references therein). The dataset consisted of the chemical data measured during the first campaign at the two sites. Data pretreatment included estimation of insoluble Ca and Mg (as difference between ED-XRF and soluble IC concentration), replacement of values below limit of detection (BDL) with 0.5*BDL and of missing values with concentration median value (Polissar et al., 1998). Few outliers, identified as those singular values showing deviations much larger than species standard deviation, were excluded. Data uncertainty for determined values was calculated according to Chow

et al. (2015). Uncertainty for missing and BDL values was calculated following Polissar (Polissar et al., 1998) and an additional 10% error was included as model uncertainty. Species category settings (generating an additional uncertainty) was based on the algorithm introduced in version 5.0 (EPA Positive Matrix Factorization 5.0 Fundamentals and User Guide). The PMF-resolved factors were assigned to aerosol sources by inspection of the species/mass reconstruction, the physical meaning and interpretability of factor profiles and the comparison with literature data on tracer compounds.

187187

Statistical Analysis

The Student's t test was conducted to check statistically significant differences of concentration of the various tracers (with $p < 0.05$) between the two sampling sites. Moreover, univariate analysis was applied by computing the Pearson correlation coefficients (R) to investigate the correlation between the factor contribution of the PMF sources at Ala and TN sites, as well as the association of OP responses with PM_{10} chemical composition.

Multivariate analysis was performed to summarize and graphically illustrate the data using Heat Map representation and hierarchical cluster analysis.

Heat Maps (HMs) are two-dimensional graphical visualization of a data set, in which data values are represented as colors; by observing the two-D spatial organization of the colors in rows and columns, visual at-a-glance multiple comparisons among data values are possible (Monti et al, 2013).

HM representation was applied to describe the source profiles of the major emission sources of PM_{10}, in such a way that each row of the grid corresponds to the single chemical tracers and each column to the PMF factors fitting the dataset. The relative amount of the analytes explained by each factor are represented by the different colors, tending toward brighter red tones for larger values.

HMs were also computed to represent multiple relationships among chemical composition and oxidative potential. In this model, each row corresponds to a day of the monitoring campaign in

Ala or TN, while each column represents a single chemical tracer or oxidative potential. The concentration data in each column were separately mean-centered and divided by their standard deviation: higher tracer values were represented with colors tending toward brighter red tones, whereas lower values tended toward brighter green tones.

Hierarchical cluster analysis (CA) was applied to the chemical components in order to discover similarities and potential correlation among the data and represent them through a dendrogram (Gordon, 1999). Distance metrics based on the Pearson correlation coefficient and the average linkage criterion were used (Gordon, 1999).

Multivariate analyses were carried out using the R software environment with the statistical packages stats, amap and gplot (R Core Team, 2016).

Results and Discussion

Levels of PM and Air Pollutants

PM_{10} mass, major, trace elements and soluble markers were daily measured at both Ala and TN sites. For each campaign the mean concentration levels and standard deviations were computed and the Student's t test applied (at the significance level $\alpha = 0.05$) to single out significant differences between the two sites (Table 1).

Although a wide temporal variability is observed during the year, in general, in the first campaign the two sites show similar values for many of the measured species, suggesting an homogenous contribution of diffuse, non-local primary sources. Overall, the most abundant ions are NO_3^- , SO_4^{2-} and NH_4^+ (~ 1500 ng m^{-3}) followed by Cl^- and Ca^{2+} (>100 ng m^{-3}) and other inorganic components at low concentration levels (< 20 ng m^{-3}). The same trend is also observed for the second campaign limited to springtime (Table 1). However, student's t test singles out some specific contribution of local emissions in Ala. In fact, the dominant element Ca (and/or its soluble form Ca^{2+}) and the analytes Cl and Zn show significantly higher mean concentrations in comparison with TN in both

campaigns, while Cu (soluble) only in the springtime (second campaign). Indeed, a remarkably number of pollution episodes causing high Cu concentration was observed at Ala in summer during the first campaign for a relatively short period (see figure S1 in Supplementary material), although this doesn't particularly alter the mean value.

Based on these outcomes, it can be inferred that some of these species are specific tracers related with direct industrial-fugitive emissions from the zinc coating process. Such a conclusion may be explained by considering that the Zn coating process of metal items is based on a hot-dip technology: the surface of pristine steel articles to be treated is overall cleaned and passivated. The items are then dipped into a molten zinc bath, either on racks or individually. Therefore, it is expected that potential emissions related with the industrial processes consist of chemicals used for de-greasing and cleaning processes, including hydrochloric acid used for de-capping, metals and chemicals released from the molten bath and possibly materials escaping from the soda-lime scrubbers and bag filters.

The higher concentration of NH_4^+ measured in Ala during the second campaign could also be due, in principle, to local fugitive emissions. Ammonia is in fact employed in the coating process. However, as NH_4^+ and NO_3^- are overall markers of secondary PM formation, it is likely that the difference observed in Ala and TN is simply due to an augmented concentration of secondary aerosol that is known to the authors to be increasingly relevant, for a number of reasons, in the southern part of the Adige valley (APPA Trento, unpublished data).

Source apportionment results

The daily speciation data collected for both sites during the first campaign were submitted to Positive Matrix Factorization in order to obtain information on source identification and apportionment. Nine sources were selected for the final solution as the PMF factors best fitting the dataset. The source profiles are described by the relative amount of the analytes explained by each factor and visually reported in detail in Figure 1 through a HM representation. In addition, the

figure shows the dendogram from Hierarchical cluster analysis in order to single out similarities among the tracers and facilitate the interpretability of the factors.

The inspection of fig. 1 allows to associate 6 factors to: (1) secondary sulphate (Sec SO_4, described by ammonium and sulphate); (2) secondary nitrate (Sec NO_3, described by ammonium and nitrate) (Seinfeld and Pandis, 2006); (3) biomass burning (BB, described by soluble K and Rb, levoglucosan, mannosan and galactosan (Hays et al., 2005; Herich et al., 2014); (4) soil resuspension/traffic (Crust Traffic, with crustal elements - Si, Al, Ca, Mg Ti - and metals - Mn, Fe, Cr, Ni, Cu - from tailpipe emissions, brake and tire wear (Thorpe et al., 2007, Val et al., 2011; Verma et al., 2015; Godoi et al., 2016; Shirmohammadi et al., 2017; Jiang et al., 2017); (5) secondary organic aerosol (SOA, identified by high loadings of oxalate); and (6) biogenic aerosol (BioA, described by arabitol, mannitol and glucose) (Bauer et al. 2008; Pietrogrande et al. 2015). As a whole, these six sources account for up to 82% of the PM_{10} mass. The seventh factor, with high loadings of Na and Mg, is supposed to represent aged sea salt particles (Aged SS) transported from the Mediterranean Sea. This hypothesis, actually under investigation, is supported by back-trajectory analyses and by the detection of V and Ni traces, likely due to ship emissions (Streibel et al. 2017). Such a spray source has been commonly identified in southern European Countries (Kishcha et al., 2012; De Cesari et al. 2014).

Finally, the eighth (Ind-Zn) and ninth (Ind-Cl) factors are attributed to direct factory emissions from the zinc coating process, as they contain mainly Zn with Ca (scrubber agent) and minor amounts of transition metals and Cl, respectively.

To support such an ascription, the weekly trend of the day-based aggregated Ind-Zn and Ind-Cl factors was investigated using non-parametric descriptive statistics and graphically depicted as boxplots (Figure S2a,b in Supplementary material). The median values of both parameters, that are significantly higher in Ala compared with the urban background site, exhibit a clear day-of-week pattern with decreased values on Sunday, which is consistent with the interruption of the industrial activities starting on Saturday at noon. The monthly-based aggregated data (not reported) reveal that

284 the median concentration of Zn in the industrial site is about constant from February to October and
285 increases in November, likely because of an augmented stagnation of pollutants in the lowest part of
286 the atmosphere. On the other hand, Cl median concentration decreases considerably during May till
287 September, although the use of hydrochloric acid as de-capping agent is possibly continued. This is
288 explained as due to the variation of partitioning of Cl into particle and gas-phase as a consequence
289 of the average ambient temperature change (Matsumoto and Tanaka, 1986).
290 To investigate the spatial distribution of the nine PMF factors, the daily contributions of each source
291 measured in Ala and TN were compared by univariate correlation analysis (Pearson correlation
292 coefficients in Table S1 in Supplementary material). For seven factors (secondary sulphate and
293 nitrate, biomass burning, soil resuspension/traffic, SOA, biogenic and aged sea salt) the
294 concentrations measured at the two sites are highly correlated, so confirming the interpretation of
295 the factors and the regional origin of these PM_{10} sources. Conversely, the factors ind-Cl and ind-Zn
296 show no correlation, confirming that the factory emissions are locally exclusive of the industrial
297 site.
298 As a final remark, it must be underlined an additional local Cu source observed at Ala during both
299 the sampling campaigns (Figure S1 in Supplementary material), but not highlighted by PMF. It
300 does not apparently scale with the other factors related with the Zn coating industry. On the other
301 hand, Cu-containing metal items are usually not coated in molten Zn bath, since their contamination
302 of liquid Zn damages the galvanizing kettles. So far, the presence of a local source of copper in Ala,
303 besides to be evident, is believed to be related with intensive organic vineyard cultivation
304 employing Cu compounds as fungicide.
305305

306 **Oxidative potential of PM_{10}**

307 OP of samples collected during the second campaign (April-May 2016) at the two sampling sites
308 was quantified by applying both DTT and AA assays: the mean and standard deviation values of the
309 whole campaign are shown in Table 1 and the temporal evolution of the measured values are shown

in Table 2 and Figure 2a, b. The DTT assay measures similar responses (OP^V_{DTT}) at both sites, ranging from a minimum of ≈ 0.2 nmol min^{-1} m^{-3} to a maximum of ≈1 nmol min^{-1} m^{-3}, with the same mean values of 0.61±0.23 nmol min^{-1} m^{-3} and 0.58±0.22 nmol min^{-1} m^{-3} at Ala and TN, respectively. On the other hand, OP^V_{AA} values show strong spatial variability with significantly higher values (Student's t test at 95% confidence level) at Ala compared with those at TN (values in bold in Table 1): OP^V_{AA} at Ala ranged from 0.1 nmol min^{-1} m^{-3} to 3.5 nmol min^{-1} m^{-3} with a mean of 1.4±1.1 nmol min^{-1} m^{-3} and those at TN are from 0.1 nmol min^{-1} m^{-3} to 1.6 nmol min^{-1} m^{-3} with a mean of 0.7±0.4 nmol min^{-1} m^{-3}.

No correlation was found between OP^V_{DTT} and OP^V_{AA} data measured at Ala (Pearson correlation coefficient R = 0.4), and only low (R = 0.7) between those at TN, despite the similarity between the values. This is consistent with our previous results (Visentin et al., 2016) and with literature data reporting different sensitivity of the two assays towards the same redox-active species present in ambient PM, although the topic is still controversial as few inter-assay comparisons have been published so far. In fact, most of the literature data highlight that DTT assay is most sensitive to organic species, including water-soluble organic carbon (WSOC) and quinones (Cho et al., 2005; Chung et al., 2006; Ayres et al. 2008; Yang et al., 2014, Verma et al., 2015), while others emphasized the role of transition metals, such as Cu and Mn (Charrier and Anastasio, 2012). Conversely, the AA assay has been shown to be most sensitive to transition metals (Janssen et al., 2014; Yang et al., 2014;Visentin et al., 2016; Fang et al., 2016), but quinone compounds may react with AA as well (Roginsky et al., 1998).

The same trend is also found using the OP^m metric related to the PM_{10} mass concentration (OP^m_{DTT} and OP^m_{AA}, Table 1): OP^m_{DTT} responses are nearly the same at the two sites, i.e., 0.06±0.03 and 0.05±0.03 nmol min^{-1} μg^{-1} at Ala and TN, respectively, while OP^m_{AA} are nearly double at Ala (0.12±0.09 nmol min^{-1} μg^{-1}) compared with TN (0.05±0.03 nmol min^{-1} μg^{-1}).

OP temporal variability

Other than differences in the measured values at the two sites, the OP^V_{DTT} and OP^V_{AA} responses show different temporal evolution of the data (Table 2 and Figure 2). In fact, OP_{DTT} was nearly homogeneously distributed during the monitoring period with small deviation around the mean, both at Ala (from 0.23 to 1.00 nmol min^{-1} m^{-3}, mean value 0.61 nmol min^{-1} m^{-3}, Fig.2a, grey full line) and TN sites (from 0.21 to 1.01 nmol min^{-1} m^{-3}, mean value 0.58 nmol min^{-1}, Fig. 2b, grey full line)**.** On the contrary, OP_{AA} shows a strong day-of-week trend characterized by the highest levels on Friday/Saturday (values in bold in Table 2). At the background TN site higher values (≥ 1 µM AA min^{-1} m^{-3}) were found close to the weekend days (Saturday 16th April, Sunday 1st May and Friday 7th May) up to the highest 1.6 µM AA min^{-1} m^{-3} on Friday 22nd April (Fig. 2b, black full line). Such a pattern is even clearer at the industry site, where the highest values close to 3 µM AA min^{-1} m^{-3} were reached on Friday, i.e., 22th and 29th April and 6th May (Fig.2a, black full line).

Such a temporal pattern is in agreement with the weekly variation of the Ind-Zn and Ind-Cl PMF factors describing local factory emissions found in the first campaign (see Figure S2a,b in Supplementary material). This suggest that the oxidative potential measured by the AA assay can be strongly related to the contributions of these trace metals showing clear temporal trends (black and gray points in the figure) (Mudway et al., 2004; Janssen et al., 2014; Fang et al., 2016; Shuster-Meiseles et al., 2016).

353353

Association of Oxidative potential with chemical components

Table 3 reports the univariate correlation analysis (Pearson coefficient, R) between the volume-normalized OP^V_{DTT} and OP^V_{AA} activity and the mass fraction of the chemical species, where the species with high correlation (R>0.60) are highlighted in bold.

In general, different patterns were observed at the two sites. OP^V values measured at the industry site are poorly correlated with most of the chemical species, with OP^V_{DTT} correlated only with potassium and rubidium (R ~ 0.8) and OP^V_{AA} almost exclusively, but very strongly, with Cu (R= 0.88). Otherwise, both OP^V_{DTT} and OP^V_{AA} at TN site were more broadly associated with aerosol

362 species, with good correlations ($R \geq 0.7$) for WSTC, SO_4, NH_4, K^+, K, Mn, Cu and Zn. In addition,
363 OP^V_{DTT} is well correlated with Rb and Pb and OP^V_{AA} with Ca, Mg and Ni.
364 These results are in agreement with several literature data that report that transition metals (e.g., Fe,
365 Mn, Cu, V, and Ni) strongly contribute to PM induced oxidative stress, since such ions stimulate
366 the production of radicals, particularly via the Fenton reaction, involved in H_2O_2 reduction (Cho et
367 al. 2005; DiStefano et al., 2009; Akhtar et al., 2010; Charrier and Anastasio, 2012, Yang et al.,
368 2014; Fang et al., 2017; Visentin et al., 2016; Shuster-Meiseles et al., 2016). In particular, the high
369 correlation of OP_{AA} with Cu found in this study at Ala is consistent with other studies reporting
370 similar high correlation coefficients (R = 0.70–0.94) when water-soluble Cu concentration is used
371 instead of elemental (total) Cu concentrations (r=0.60–0.76 in other studies) (Janssen et al., 2014;
372 Fang et al., 2016).
373 Heat Maps were computed on the data set in order to highlight relationships among the oxidative
374 potential and chemical composition of PM samples: two individual models include OP^V_{DTT} and
375 OP^V_{AA} separately (Figure 3a,b) (Gordon, 1999; Monti et al, 2013). Within the general similarity of
376 most of the measured concentrations, a visual inspection of the obtained Heat Maps singles out that
377 in some days some analytes have higher levels at Ala compared with TN, in particular the
378 anidrosugars (Levo, Mann and Gal) and the metals Cu and Zn (brighter red tones of the
379 corresponding pixels). At both sites, most analytes show a similar temporal trend with maximum
380 levels close to Friday 22nd April, as the total PM_{10} mass. In addition, a more pronounced day-of-
381 week evolution was observed for Ala data, that are characterized by the highest levels on
382 Friday/Saturday days, i.e., 22nd and 29th April and 7th May. Concerning the OP^{DTT}_V and OP^{AA}_V
383 values measured at the two sampling sites, the heat maps highlight the general similarity of the DTT
384 assay responses (Fig 3a) and the strong spatial variability of $OP_{AA,}$ with higher values measured at
385 Ala site compared to those at TN (Fig 3b). Moreover, it is clearly visible the day-of-week trend of
386 OP^{AA}_Vvalues at Ala site.

The trend was further investigated by hierarchical cluster analysis (dendrograms in the upper side of the HMs in Figure 3a,b). The dendrogram of the dataset including the OP_{DTT} shows that these values are closest to K^+ and Rb group and then it is included in a larger group formed by Mg^{2+}, Pb, SO_4^{2-},WSTC and Mn also Sr, Fe, Ca^{2+}, NH_4^+ and NO_3^- (Figure 3a). This finding may indicate a possible relation of DTT activity with a combination of different contributions, including primary emissions, such as biomass burning (K and Rb) and traffic (Fe, Pb, Ca, Mg, Mn), and also to secondary particle formation (SO_4^{2-}). The impact of vehicular traffic emissions on DTT activity has been recently reported in freeway environments as attributable to emissions of fuel combustion and lube oil as well as to vehicular abrasion processes, especially from brake and tirewear abrasion (Li et al., 2009; Val et al., 2011; Charrier et al., 2015; Godoi et al., 2016; Shirmohammadi et al., 2017). Otherwise, cluster analysys of the dataset including OP_{AA} classifies Cu as the closest species to OP_{AA}, followed by Zn, and this cluster is then close to a wide group of chemical components, including Al, K, Rb, Ca and Mg elements (Figure 3b). Consistently with the above reported results, these data confirm that OP_{AA} activity is dominated by the contributions of metals, despite their low fractions in ambient aerosols over other more abundant species (Charrier and Anastasio, 2012; Charrier et al., 2015; Visentin et al., 2016). According to the results of the PMF model, Zn, with Ca and minor amounts of transition metals, are the main components of direct emissions from the zinc factory (ind-Zn), while other metals are mainly attributed to the soil resuspension/traffic factor. Additionally, high concentrations of copper in Ala are explained by its use in vineyard cultivation.

Conclusions

This study tried to assess the impact of metal rich atmospheric particulate on ambient air quality, with specific concern on capability of PM to produce oxidative stress, as most likely mechanism of adverse health effects of PM.

The reported results clearly show that few selected metals, mainly Zn and Cu, strongly enhance PM oxidative potential, even if they only weakly impacted PM_{10} mass concentration and chemical composition. These metals are emitted by the anthropogenic activities carried out in the investigated area, mainly a zinc coating industry in combination with traffic in a congested major motorway and widespread pesticide use in the surrounding vineyards.

Concerning the still open question of different sensitivity of the DTT and AA assays, our results may be considered an experimental proof of the highest sensitivity of AA assay towards transition metals.

Consequently, the combination of the two approaches can strengthen each other in giving insight into the contribution of chemical composition to oxidative properties of PM. This stresses once again the importance of an in-depth chemical speciation of particulate matter.

As a general conclusion, the results of this study are useful in providing insight into the relative contribution of toxicologically-relevant components, that is vital in designing a more straight-forward approach to air quality management and emission control technologies focused on specific components and sources, rather than on PM mass concentration which is currently used for air quality legislation.

Funding

This work was supported by the Fund for the Scientific Research of the University of Ferrara [FAR 2017].

References

Antiñolo, M., Willis, M. D., Zhou, S., and Abbatt, J. P., 2015. Connecting the oxidation of soot to its redox cycling abilities. Nature Communications 6, 6812. doi:10.1038/ncomms7812.

438 Akhtar, U.S., McWhinney, R.D., Rastogi, N., Abbatt, J.P., Evans, G.J., Scott, J.A., 2010. Cytotoxic
439 and proinflammatory effects of ambient and source-related particulate matter (PM) in relation to the
440 production of reactive oxygen species (ROS) and cytokine adsorption by particles. Inhalation
441 Toxicology 22, 37-47.
442 Ayres, J.G., Borm, P., Cassee, F.R., Castranova, V., Donaldson, K., Ghio, A., Harrison, R.M.,
443 Hider, R., Kelly, F., Kooter, I.M., Marano, F., Maynard, R.L., Mudway, I., Nel, A., Sioutas, C.,
444 Smith, S., Baeza-Squiban, A., Cho, A., Duggan, S., Froines, J., 2008. Evaluating the toxicity of
445 airborne particulate matter and nanoparticles by measuring oxidative stress potential: workshop
446 report and consensus statement. Inhalation Toxicology 20, 75-99.
447 Bates, J.T., Weber, R.J., Abrams, J., Verma, V., Fang, T., Klein, M., Strickland, M.J., Sarnat, S.E.,
448 Chang, H.H., Mulholland, J.A., Tolbert, P.E., Russell, A.G., 2015. Reactive oxygen species
449 generation linked to sources of atmospheric particulate matter and cardiorespiratory effects.
450 Environmental Science & Technology 49, 13605-13612.
451 Bauer, H., Claeys, M., Vermeylen, R., Schueller, E., Weinke, G., Berger, A., Puxbaum, H., 2008.
452 Arabitol and mannitol as tracers for the quantification of airborne fungal spores. Atmospheric
453 Environment 42, 588–593.
454 Belis, C.C., Larsen, B.R., Amato, Zadad, I.E., Favez, O., Harrison, R.M., Hoplke, P.K., Nava, S.,
455 Paatero, P., Prévôt, A., Quass, U., Vecchi, R., Viana M., 2014. European Guide on Air Pollution
456 Source Apportionment with Receptor Models. Publications Office of the European Union.
457 Publications Office of the European Union. ISBN: 978-92-79-32514-4 (print),978-92-79-32513-7
458 (pdf).
459 Brook, R.D., Rajagopalan, S., Pope, C.A., Brook, J.R., Bhatnagar, A., Diez-Roux, A.V., Holguin,
460 F., Hong, Y., Luepker, R.V., Mittleman, M.A., Peters, A., Siscovick, D., Smith, S.C., Whitsel, L.,
461 Kaufman, J.D., 2010. Particulate matter air pollution and cardiovascular disease. Circulation 121,
462 2331-2378.

463 Charrier, J.G., Anastasio, C., 2012. On dithiothreitol (DTT) as a measure of oxidative potential for
464 ambient particles: evidence for the importance of soluble transition metals. Atmospheric Chemistry
465 and Physics 12, 11317-11350.
466 Charrier, J.C., Richards-Henderson, N.K., Bein, K.J., McFall, A.S., Wexler, A.S., Anastasio, C.,
467 2015. Oxidant production from source-oriented particulate matter - Part 1: Oxidative potential using
468 the dithiothreitol (DTT) assay. Atmospheric Chemistry and Physics 15, 2327–2340.
469 Chen, Y., Ebenstein, A., Greenstone, M., and Li, H., 2013. Evidence on the impact of sustained
470 exposure to air pollution on life expectancy from China's Huai River policy. Proceedings of the
471 National Academy of Science of the United States of America 110, 12936-12941.Cho, A.K.,
472 Sioutas, C., Miguel, A. H., Kumagai, Y., Schmitz, D.A., Singh, M., Eiguren-Fernandez, A.,
473 Froines, J.R., 2005. Redox activity of airborne particulate matter at different sites in the Los
474 Angeles Basin. Environmental Research 99, 40-47.
475 Chow, J.C., Lowenthal, D.H., Chen, L.-W.A., Wang, X., Watson, J.G., 2015. Mass reconstruction
476 methods for $PM_{2.5}$: a review. Air Quality, Atmosphere & Health Health 8, 243–263.
477 Chung, M.Y., Lazaro, R.A., Lim, D., Jackson, J., Lyon, J., Rendulic, D., Hassom, A.S., 2006.
478 Aerosol-borne quinones and reactive oxygen species generation by particulate matter extracts.
479 Environmental Science & Technology 40, 4880-4886.
480 Crobeddu, B., Aragao-Santiago, L., Bui, L.C., Boland,S., Baeza Squib, A., 2017. Oxidative
481 potential of particulate matter 2.5 as predictive indicator of cellular stress. Environmental Pollution
482 230 125-133.
483 Davidson, C.I., Phalen, R.F., Solomon, P.A., 2005. Airborne particulate matter and human health: a
484 review. Aerosol Science and Technology 39, 737-749.
485 De Cesari, D., Genga, A., Ielpo, P., Siciliano, M., Mascolo, G., Grasso, F.M., Contini, D., 2014.
486 Source apportionment of $PM_{2.5}$ in harbor-industrial area of Brindisi (Italy). Identification and
487 estimation of the contribution of inport ship emissions. Science of the Total Environment 497-498,
488 392-400.

DiStefano, E., Eiguren-Fernandez, A., Delfino, R.J., Sioutas, C., Froines, J.R., Cho, A.K., 2009. Determination of metal-based hydroxyl radical generating capacity of ambient and diesel exhaust particles. Inhalation Toxicology 21, 731–738.

EPA: https://www.epa.gov/air-research/positive-matrix-factorization-model-environmental-data-analyses.

Fang T., Verma V., Bates J.T., Abrams J., Klein M., Strickland M.J., Sarnat S.E., Chang H.H., Mulholland J.A., Tolbert P.E., Russell A.G., Weber R.J., 2016. Oxidative potential of ambient water-soluble $PM_{2.5}$ in the southeastern United States: contrasts in sources and health associations between ascorbic acid (AA) and dithiothreitol (DTT) assays. Atmospheric Chemistry and Physics 16, 3865-3879.

Fang T., Guo, H., Zeng, L., Verma V., Nenes, A.., Weber R.J., 2017. Highly Acidic Ambient Particles, Soluble Metals, and Oxidative Potential: A Link between Sulfate and Aerosol Toxicity. Environmental Science & Technology 51, 2611−2620

Godoi, R.H.M., Polezer, G., Borillo,G.C., Brown, A., Valebona, F.B., Silva, T.O.B., Ingberman, A.B.G., Nalin, M., Yamamoto, C.I., Potgieter-Vermaak, S., Renato A. Penteado Neto, R.A.P., de Marchi, M.R., Saldiva, P.H.N, Pauliquevis, T., Godoi, A.F.L., 2016. Influence on the oxidative potential of a heavy-duty engine particle emission due to selective catalytic reduction system and biodiesel blend. Science of the Total Environment 560–561, 179–185.

Gordon, A. D., 1999. Classification, 2nd ed.; Chapman and Hall/CRC; Boca Raton, FL.

Hays, M.D., Fine, P.M., Geron, C.D., Kleeman, M.J., Gullett, B.K., 2005. Open burning of agricultural biomass: physical and chemical properties of particle-phase emissions. Atmospheric Environment 39, 6747-6764.

Hedayat, F., Stevanovic, S., Miljevic, B., Bottle, S., and Ristovski, Z., 2014. Review-evaluating the molecular assays for measuring the oxidative potential of particulate matter. Chemical Industry and Chemical Engineering Quarterly. 21, 201-210.

514 Herich, H., Gianini, M.F.D., Piot, C., Mocnik, G., Jaffrezo J.L., Besombes, J.L., Prévôt, A.S.H.,
515 Hueglin, C., 2014. Overview of the impact of wood burning emissions on carbonaceous aerosols
516 and PM in large parts of the Alpine region. Atmospheric Environment 89, 64-75.
517 Kishcha, P., Starobinets, B, Udisti, R., Becagli, S., di Sarra, A., Sferlazzo, D., Bommarito, C.,
518 Alpert, P., 2012. Sea-Salt Aerosol Mass Concentration Oscillations after Rainfall, Derived from
519 Long-Term Measurements in Lampedusa (Central Mediterranean). 2012 International Scholarly
520 Research Network ISRN Meteorology, Article ID 679120, 8pages,
521 http://dx.doi.org/10.5402/2012/679120.
522 Li, N., Kim S, Wang, M., Froines, J., Sioutas, C., Nel, A., 2002. Use of a stratified oxidative stress
523 model to study the biological effects of ambient concentrated and diesel exhaust particulate matter.
524 Inhalation Toxicology 14, 459–486.
525 Li, N., Xia, T., Nel, A. E., 2008. The role of oxidative stress in ambient particulate matter-induced
526 lung diseases and its implications in the toxicity of engineered nanoparticles. Free Radical Biology
527 and Medicine 44, 1689-1699.
528 Li Q., Wyatt, A., Kamens, R.M., 2009. Oxidant generation and toxicity enhancement of aged-diesel
529 exhaust. Atmospheric Environment 43, 1037-1042.
530 Jansen, K.L., Larson, T.V., Koenig, J Q., Mar, T F., Fields, C., Stewart, J., Lippmann, M., 2005.
531 Associations between health effects and particulate matter and black carbon in subjects with
532 respiratory disease. Environmental Health Perspectives 113, 1741-1746.
533 Janssen, N.A.H., Yang, A., Strak, M., Steenhof, M., Hellack, B., Gerlofs-Nijland, M.E.,
534 Kuhlbusch, T., Kelly, F., Harrison, R., Brunekreef, B., Hoek, G., Cassee, F., 2014. Oxidative
535 potential of particulate matter collected at sites with different source characteristics. Science Total
536 Environment 472, 572-581.
537 Jiang, H., Jang, M., Yu, Z., 2017. Dithiothreitol activity by particulate oxidizers of SOA produced
538 from photooxidation of hydrocarbons under varied NOx levels. Atmospheric Chemistry and
539 Physics 17, 9965-9977.

Matsumoto, K., Tanaka, H., 1996. Formation and dissociation of atmospheric particulate nitrate and cloride: an approach based on phase equilibria. Atmospheric Environment 30, 639- 648.

Monti, F., Dell'Anna, R., Sanson, A., Fasoli, M., Pezzotti, M., Zenoni, S., 2013. A multivariate statistical analysis approach to highlight molecular processes in plant cell walls through ATR FT-IR microspectroscopy: The role of the α-expansin PhEXPA1 in Petunia hybrid. Vibrational Spectroscopy 65, 36-43.

Mudway, I.S., Stenfors, N., Duggan, S.T., Roxborough, H., Zielin-ski, H., Marklund, S.L., Blomberg, A., Frew, A.J., Sandstrom, T., Kelly, F.J., 2004. An in vitro and in vivo investigation of the effects of diesel exhaust on human airway lining fluid antioxidants. Archives of Biochemistry and Biophysics 423, 200–212.

Paatero P., Tapper U., 1994. Positive matrix factorization: a non-negative factor model with optimal utilization of error estimates of data values. Environmetrics 5, 111-126.

Perrino, C., Catrambone, M., Dalla Torre, S., Rantica, E., Sargolini, T., Canepari, S., 2014. Seasonal variations in the chemical composition of particulate matter: a case study in the Po Valley. Part I: macro-components and mass closure. Environmental Science Pollution Research 21, 3999–4009.

Peters, A., Veronesi, B., Calderón-Garcidueñas, L., Gehr, P., Chen, L. C., Geiser, M., Reed, W., Rothen-Rutishauser, B., Schürch, S., Schulz, H., 2006. Translocation and potential neurological effects of fine and ultrafine particles a critical update. Particle and Fibre Toxicology 3:13, https://doi.org/10.1186/1743-8977-3-13.

Pietrogrande, M.C., Bacco, D., Ferrari, S., Kaipainen, J., Ricciardelli, I., Riekkola, M-J., Trentini, A., Visentin, M., 2015. Polar organic marker compounds in atmospheric aerosol in the Po valley during the Supersito campaigns - Part 3: Contribution of wood combustion to wintertime atmospheric aerosols in Emilia Romagna region (Northern Italy). Atmospheric Environment 122, 291-305.

565 Polissar, A.V., Hopke P.K., Paatero P., Malm W.C., Sisler J.F., 1998. Atmospheric aerosol over
566 Alaska 2. Elemental composition and sources. Journal of Geophysical Research D: Atmospheres
567 103 (D15), 19045-19057.
568 R Core Team, R Foundation for Statistical Computing, 2016. http://www.R-project.org, accessed:
569 28.03.2017.
570 Roginsky, V.A., Barsukova, T.K., Bruchelt, G., Stegmann, H.B., 1998. Kinetics of redox
571 interaction between substitutes 1,4-benzoquinones and ascorbate under aerobic conditions: Critical
572 phenomena. Free Radical Research 29, 115-125.
573 Saffari, A., Daher, N., Shafer, M.M., Schauer, J.J., Sioutas, C., 2014. Global Perspective on the
574 Oxidative Potential of Airborne Particulate Matter: A Synthesis of Research Findings.
575 Environmental Science & Technology 2014, 48, 7576−7583
576 Sandrini S., Fuzzi, S., Piazzalunga, A., Prati, P., Bonasoni, Cavalli, F., Bove M.C., Calvello, M.,
577 Cappelletti, D., Colombi, C., Contini, D., de Gennaro, G., Di Gilio, A., Fermo, P., Ferrero, L.,
578 Gianelle, V., Giugliano, M., Ielpo, P., Lonati, G., Marinoni, A., Massabò, M., Molteni, U., Moroni,
579 B., Pavese, G., Perrino, C., Perrone, M.G., Perrone, M.R., Putaud, J.P., Sargolini, T., Vecchi, R.,
580 Gilardoni, S., 2014. Spatial and seasonal variability of carbonaceous aerosol across Italy.
581 Atmospheric Environment 99, 587-598.
582 Seinfeld, J.H., Pandis, S.N., 2006. Atmospheric Chemistry and Physics: from Air Pollution to
583 Climate Change. second ed. Wiley, New York. ISBN 978-0-471-72018-8.
584 Shuster-Meiseles, M., Shafer, M.M., Heo, J., Pardo, M., Antkiewicz, D.S., Schauer, J.J., Rudich,
585 A., Rudichet, Y., 2016. ROS-generating/ARE-activating capacity of metals in roadway particulate
586 matter deposited in urban environment. Environmental Research 146, 252–262.
587 Shirmohammadi, F., Wang, D., Hasheminassab, S., Verma, V., Schauer, J.J., Shafer, M.M., Sioutas,
588 C., 2017. Oxidative potential of on-road fine particulate matter ($PM_{2.5}$) measured on major freeways
589 of Los Angeles, CA, and a 10-year comparison with earlier roadside studies. Atmospheric
590 Environment 148, 102-114.

591 Streibel, H., Schnelle-Kreis, J., Czech, H., Harndorf, H., Jakobi, G., Jokiniemi, J., Karg, E.,
592 Lintelmann, J., Matuschek, G., Michalke, B., Müller, L., Orasche, J., Passig, J., Radischat, C.,
593 Rabe, R., Reda, A., Rüger, C., Schwemer, T., Sippula, O., Stengel, B., Sklorz, M., Torvela, T.,
594 Weggler, B., Zimmermann, R., 2017. Aerosol emissions of a ship diesel engine operated with diesel
595 fuel or heavy fuel oil. Environmental Science and Pollution Research 24, 10976–10991.
596 Thorpe, A.J., Harrison, R.M., Boulter, P.G., McCrae, I.S., 2007. Estimation of particle resuspension
597 source strength on a major London Road. Atmospheric Environment 41, 8007-8020.
598 Val, S., Martinon, L., Cachier, H., Yahyaoui, A., Marfaing, H., Baeza-Squiban, A., 2011. Role of
599 size and composition of traffic and agricultural aerosols in the molecular responses triggered in
600 airway epithelial cells. Inhalation Toxicology 23, 627-640.
601 Verma, V., Fang, T., Xu, L., Peltier, R.E., Russell, A.G., Ng, N.L., Weber, R.J., 2015. Organic
602 aerosols associated with the generation of reactive oxygen species (ROS) by water-soluble $PM_{2.5}$.
603 Environmental Science & Technology 49, 4646-4656.
604 Visentin, M., Pagnoni, A., Sarti, E., Pietrogrande, M.C., 2016. Urban $PM_{2.5}$ oxidative potential:
605 Importance of chemical species and comparison of two spectrophotometric cell-free assays.
606 Environmental Pollution 219, 72-79.
607 Yang, A., Jedynska, A., Hellack, B., Kooter, I., Hoek, G., Brunekreef, B., Kuhlbusch, T.A.J.,
608 Cassee, F.R., Janssen, N.A.H., 2014. Measurement of the oxidative potential of $PM_{2.5}$ and its
609 constituents: the effect of extraction solvent and filter type. Atmospheric Environment 83, 35-42.
610610

Figure captions

Figure 1: Heat Map of PMF model of the dataset of the first monitoring campaign. Rows correspond to the single chemical tracers daily measured; columns represent the the source profiles of the 9 PMF factors best fitting the dataset. The upper side of the figures reports the dendrograms computed on the data set.

Figure 2: temporal evolution of the parameters measured at Ala (2a) and Trento sites (2b): full black line: OP^V response of AA assay, OP_{AA}; dotted black line; mean OP_{AA} value; full grey line: response of DTT assay, OP_{DTT}; dotted grey line: mean OP_{DTT} value; black dashed line: Zn concentration; grey dashed line: Cu concentration.

Figure 3: Heat Maps of the data measured in Ala and TN sites during the second monitoring campaign. Rows correspond to the campaign days, columns represent single chemical tracers or oxidative potential. The upper side of the figures reports the dendrograms computed on the two data sets, including OP_{AA} and OP_{DTT} separately.

Figure 3a: data matrix including OP^V_{DTT} values; Figure 3b: data matrix including OP^V_{AA} values.

629 **Table 1**. Concentration data measured during both sampling campaigns, means and standard
630 deviation. **Means** with significant differences (Student t-test), v*alues* indicate the soluble fraction of
631 the metal. Units: PM (μg m^{-3}); remaining analytes (ng m^{-3}); OP^V (nmol min^{-1} m^{-3}); OP^m [(mol min^{-1}
632 μg^{-1}).
633

	1st campaign				2nd campaign			634
	Ala		TN		Ala		TN	
	Mean	SD	Mean	SD	Mean	SD	Mean	SD
PM	20.3	10.8	19.0	10.0	14.7	10.1	12.7	7.7
Cl^-	**158.5**	**237.6**	**45.3**	**109.3**	**95.1**	**97.0**	**25.4**	**25.1**
NO_3^-	2432.9	3085.0	2056.9	3529.2	**2595.1**	**3633.9**	**959.0**	**1031.7**
SO_4^{2-}	1769.1	1343.5	1756.5	1387.5	1584.3	1140.8	1099.7	805.5
NH_4^+	1055.4	1010.2	1031.8	1169.4	**1040.6**	**924.2**	**593.1**	**415.0**
Na^+	109.2	132.7	109.6	117.4	116.1	112.9	83.5	100.8
K^+	130.0	86.8	153.6	118.4	88.3	57.3	60.5	26.8
Mg^{2+}	39.1	24.6	47.8	26.9	41.5	32.9	37.5	23.0
Ca^{2+}	**454.4**	**291.3**	**328.8**	**195.5**	**474.3**	**455.1**	**237.9**	**169.7**
Arabitol	23.5	80.8	23.9	20.7	13.9	4.5	11.3	6.1
Mannitol	24.0	79.7	26.1	23.5	11.9	4.5	9.9	5.1
Levoglucosan	131.7	187.7	143.0	188.0	52.2	31.4	37.7	21.7
Mannosan	14.1	84.7	22.3	26.3	6.0	4.3	4.7	2.8
Galactosan	1.9	81.1	7.6	10.3	2.5	1.7	1.6	0.9
Glucose	27.4	80.9	30.7	27.4	26.9	13.5	23.1	13.2
Al	139.8	117.1	149.3	134.2	*1.6*	*2.8*	*0.4*	*0.8*
Ca	**685.9**	**455.9**	**488.3**	**321.8**				
Fe	480.2	256.0	427.4	216.9	*7.2*	*7.4*	*4.5*	*4.9*
Mg	73.3	53.9	69.8	44.6				
K	245.7	145.0	256.2	159.9				
Cr	4.5	1.7	4.5	1.8	*0.61*	*0.40*	*0.50*	*0.35*
Mn	8.8	4.4	8.1	3.7	*3.42*	*2.36*	*2.46*	*1.31*
Ni	2.4	0.9	2.1	0.7	*0.36*	*0.38*	*0.18*	*0.13*
Pb	3.1	2.6	3.6	3.3	*0.31*	*0.33*	*0.23*	*0.23*
Cu	16.7	17.9	13.4	7.7	***8.4***	***7.9***	***3.5***	***3.0***
Rb	0.6	0.5	0.7	0.5	*0.13*	*0.08*	*0.12*	*0.17*
Zn	**87.0**	**60.4**	**23.3**	**14.1**	***24.5***	***16.4***	***6.2***	***4.3***
Si	371.9	368.0	378.8	367.5				
Ti	13.7	9.0	15.1	10.1				
Sr					*0.93*	*1.15*	*0.53*	*0.33*
V					*0.55*	*0.88*	*0.25*	*0.29*
S	1082.4	1030.8	1076.8	1048.3				
Oxalate	172.9	140.3	138.9	184.1				
insoluble Ca	155.3	137.7	160.9	160.7				
insoluble Mg	26.4	37.5	22.4	34.6				
WSTC					1345.9	595.9	1176.9	516.1
OP^v_{DTT}					0.61	0.23	0.58	0.22
OP^V_{AA}					**1.4**	**1.1**	**0.7**	**0.4**
OP^m_{DTT}					0.06	0.03	0.05	0.03
OP^m_{AA}					**0.12**	**0.09**	**0.05**	**0.03**

635 **Table 2**: temporal evolution of OP^{V}_{DTT} and OP^{V}_{AA} measured at the two sampling sites. **OP^{V}**
636 **responses** measured on Friday/Saturday/Sunday

		Ala		TN	
Date	Week day	OP^{V}_{DTT} (nmol min^{-1} m^{-3})	OP^{V}_{AA} (nmol min^{-1} m^{-3})	OP^{V}_{DTT} (nmol min^{-1} m^{-3})	OP^{V}_{AA} (nmol min^{-1} m^{-3})
06/04/2016	wed	1.00	0.94	1.01	1.00
07/04/2016	thu	0.98	0.76	0.52	0.71
08/04/2016	**fri**	**0.63**	**0.42**	**0.28**	**0.26**
09/04/2016	**sat**	**0.26**	**0.36**	**0.64**	**0.46**
14/04/2016	thu	0.31	1.45	0.28	0.26
16/04/2016	**sat**	**0.27**	**0.11**	**0.45**	**1.00**
20/04/2016	wed	0.58	2.08	0.39	0.48
21/04/2016	thu	0.59	2.48	0.66	1.04
22/04/2016	**fri**	**0.80**	**2.64**	**0.83**	**1.56**
24/04/2016	sun	0.67	0.64	0.21	0.00
25/04/2016	mon	0.35	0.06	0.25	0.12
26/04/2016	tue	0.74	0.60	0.64	0.50
28/04/2016	thu	0.79	3.34	0.47	0.79
29/04/2016	**fri**	**0.91**	**3.54**	**0.71**	**0.38**
30/04/2016	**sat**	**0.86**	**1.02**	**0.61**	**0.34**
01/05/2016	**sun**	**0.53**	**0.44**	**0.85**	**1.11**
03/05/2016	tue	0.54	0.92	0.70	0.45
04/05/2016	wed	0.31	1.08	0.29	0.24
05/05/2016	thu	0.23	1.04	0.55	0.74
06/05/2016	**fri**	**0.79**	**3.41**	**0.79**	**1.00**
07/05/2016	**sat**	**0.61**	**2.45**	**0.78**	**1.05**
08/05/2016	sun	0.62	1.31	0.71	0.69
09/05/2016	mon	0.68	1.45	0.68	1.44

637 **Table 3**: Association between Oxidative Potential, measured with DTT and AA assays, and
638 concentration data measured during the second campaign (April-May 2016) at Ala and TN sites:
639 Pearson correlation coefficients (R).
640

	Ala		TN	
	OP^{v}_{DTT} (nmol min^{-1} m^{-3})	OP^{v}_{AA} (nmol min^{-1} m^{-3})	OP^{v}_{DTT} (nmol min^{-1} m^{-3})	OP^{v}_{AA} (nmol min^{-1} m^{-3})
	R	R	R	R
PM	0.52	0.55	0.46	0.62
WSTC	0.57	0.60	**0.73**	**0.76**
Cl^-	0.09	0.09	0.17	0.08
NO_3^-	0.40	0.36	0.45	0.59
SO_4^{2-}	0.47	0.46	**0.70**	**0.82**
NH_4^+	0.46	0.43	**0.67**	**0.78**
Na^+	0.32	0.26	0.24	0.28
K^+	**0.77**	0.55	**0.84**	**0.71**
Mg^{2+}	0.57	0.46	0.62	**0.73**
Ca^{2+}	0.52	0.57	0.57	**0.79**
Arabitol	0.51	0.58	0.33	0.42
Mannitol	0.50	0.69	0.47	0.53
Levoglucosan	0.58	0.10	0.52	0.07
Mannosan	0.42	0.03	0.41	-0.10
Galactosan	0.42	0.02	0.41	-0.06
Glucos	0.11	0.10	0.33	0.35
Al sol	0.25	0.05	0.35	0.52
Ca sol	0.50	0.55	0.55	**0.78**
Fe sol	0.38	0.35	0.60	0.41
Mg sol	0.56	0.44	0.61	**0.72**
K sol	**0.75**	0.51	**0.79**	**0.72**
Na sol	0.19	0.30	0.24	0.29
Cr sol	-0.06	0.12	-0.13	0.05
Mn sol	0.61	0.51	**0.68**	**0.73**
Ni sol	0.36	0.17	0.41	**0.74**
Pb sol	0.30	0.27	**0.68**	0.53
Cu sol	0.58	**0.88**	**0.69**	**0.77**
Rb sol	**0.83**	0.48	**0.85**	0.61
Sr sol	0.41	0.21	0.45	**0.75**
V sol	0.09	-0.09	0.23	0.61
Zn sol	0.51	0.59	**0.68**	**0.70**
OP^{v}_{DTT}	1.00	0.60	1.00	0.71

641

Graphical Abstract (for review)

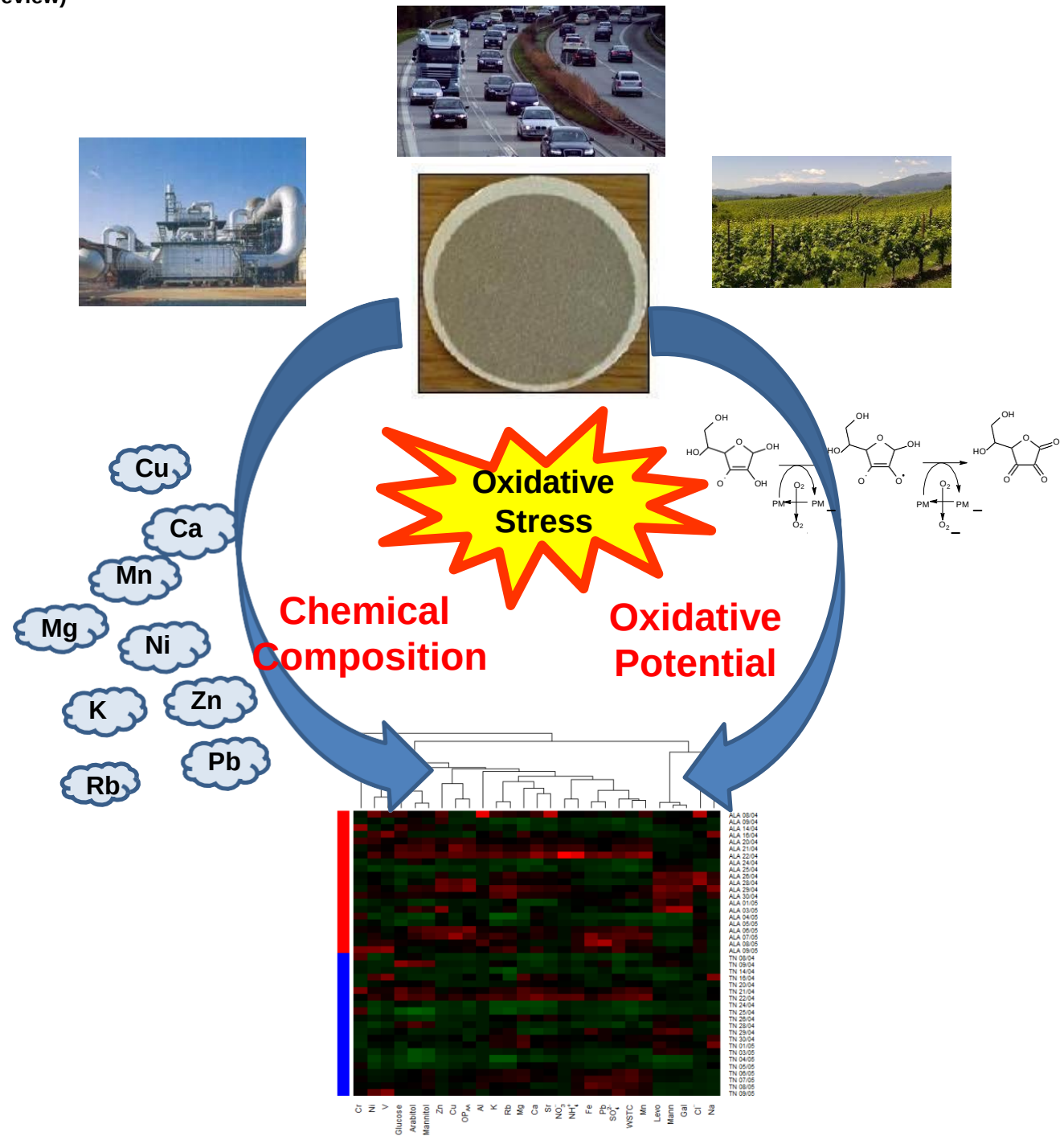

Highlights

- Chemical composition of atmospheric aerosol influences its oxidative potential
- Airborne metals are mainly mitted from zinc coating industry, traffic and agricultural activity
- Two cell-free assays give complementary information on aerosol oxidative potential
- Responses of ascorbic acid assay are higher at the industrial site, mainly associated with copper
- Responses of dithiothreitol assay are associated with several chemical tracers at both sites.

Figure 1

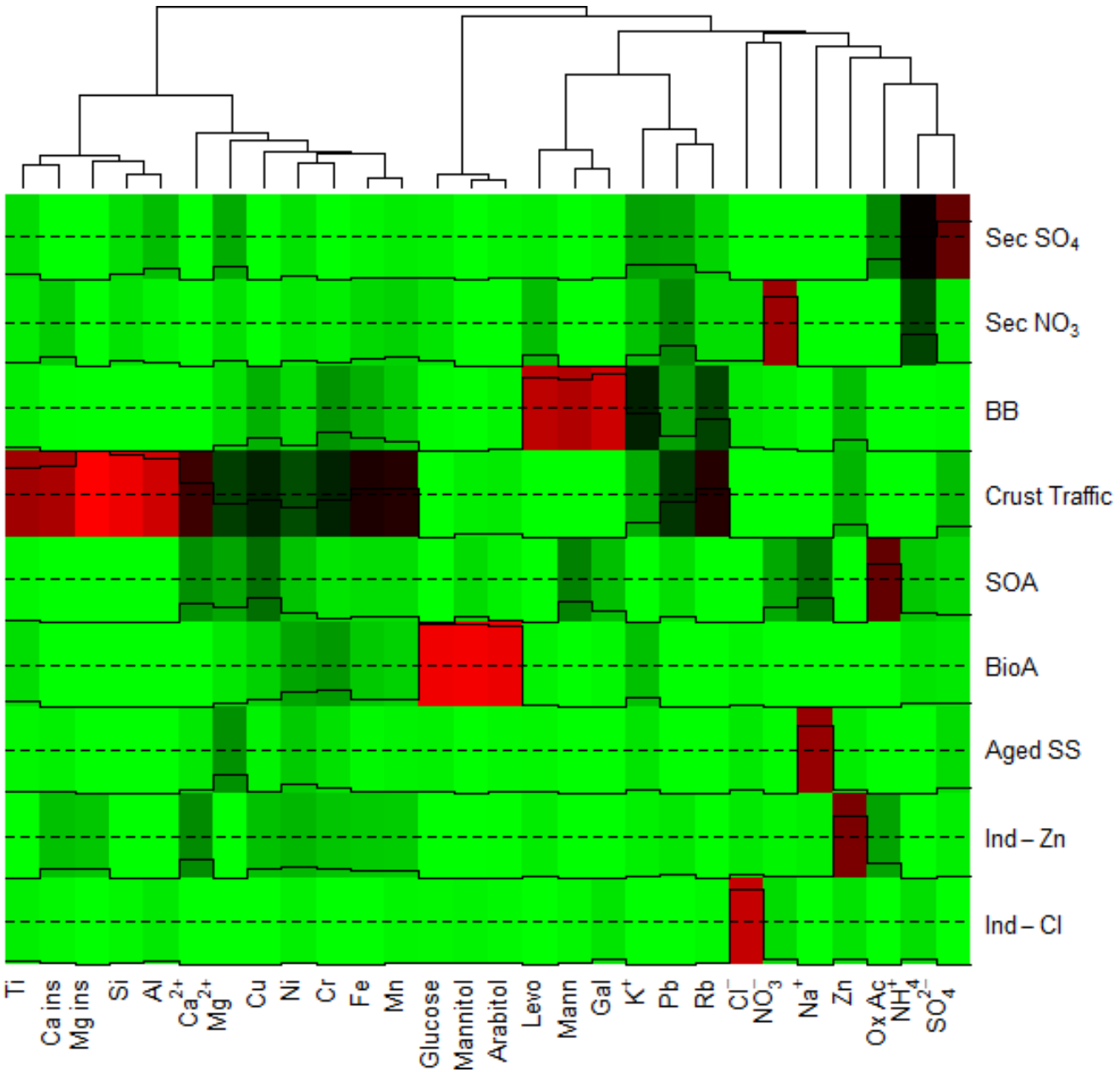
Sec SO_4
Sec NO_3
BB
Crust Traffic
SOA
BioA
Aged SS
Ind – Zn
Ind – Cl
Ti
Ca ins
Mg ins
Si
Al
Ca^{2+}
Mg^{2+}
Cu
Ni
Cr
Fe
Mn
Glucose
Mannitol
Arabitol
Levo
Mann
Gal
K^+
Pb
Rb
Cl^-
NO_3^-
Na^+
Zn
Ox Ac
NH_4^+
SO_4^{2-}

Figure 2

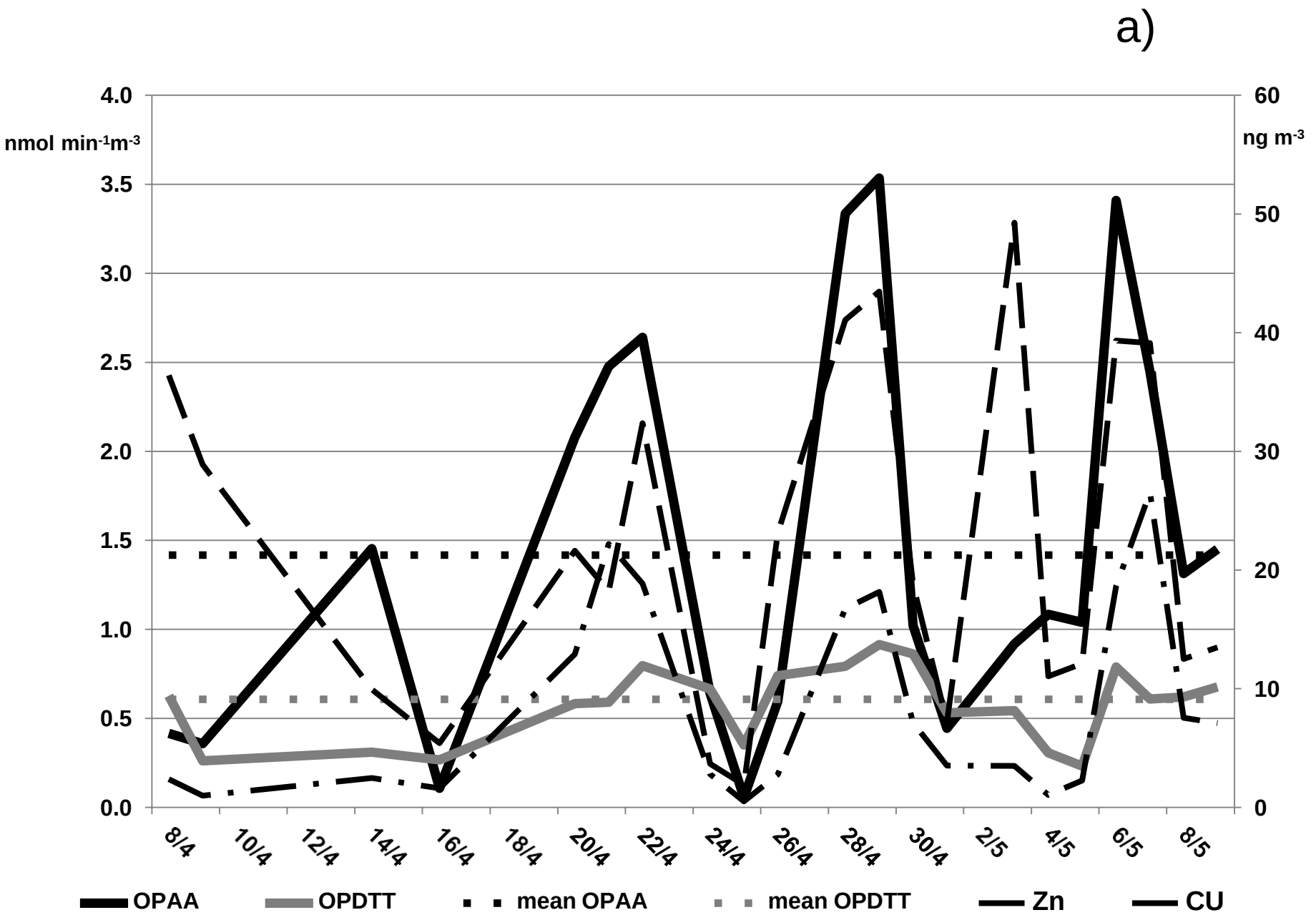
a)
4.0
3.5
3.0
2.5
2.0
1.5
1.0
0.5
0.0
nmol min-1m-3
60
50
40
30
20
10
0
ng m-3
8/4
10/4
12/4
14/4
16/4
18/4
20/4
22/4
24/4
26/4
28/4
30/4
2/5
4/5
6/5
8/5
OPAA
OPDTT
mean OPAA
mean OPDTT
Zn
CU

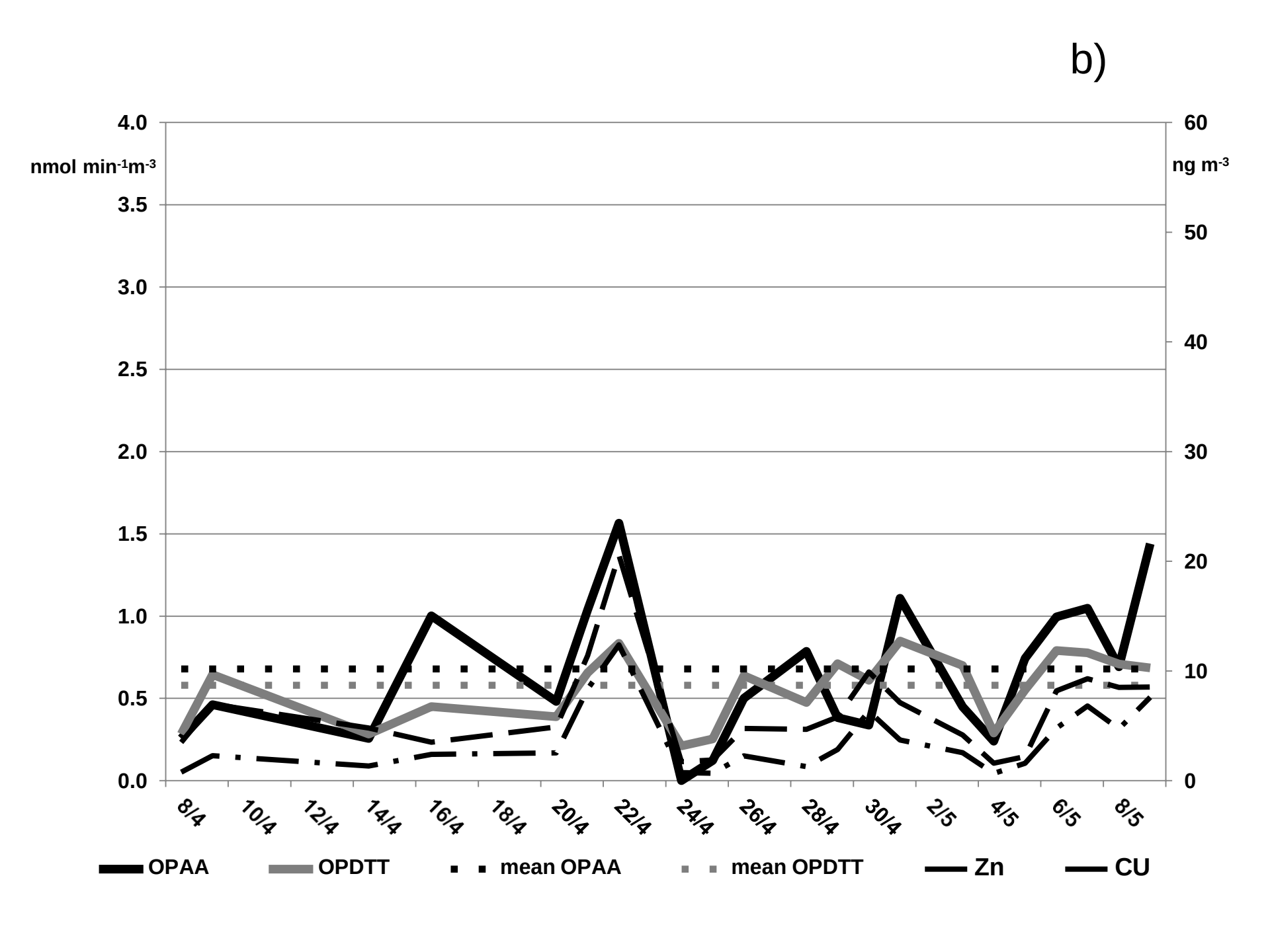
b)
4.0
nmol min-1m-3
3.5
3.0
2.5
2.0
1.5
1.0
0.5
0.0
60
ng m-3
50
40
30
20
10
0
8/4
10/4
12/4
14/4
16/4
18/4
20/4
22/4
24/4
26/4
28/4
30/4
2/5
4/5
6/5
8/5
OPAA
OPDTT
mean OPAA
mean OPDTT
Zn
CU

Figure 3

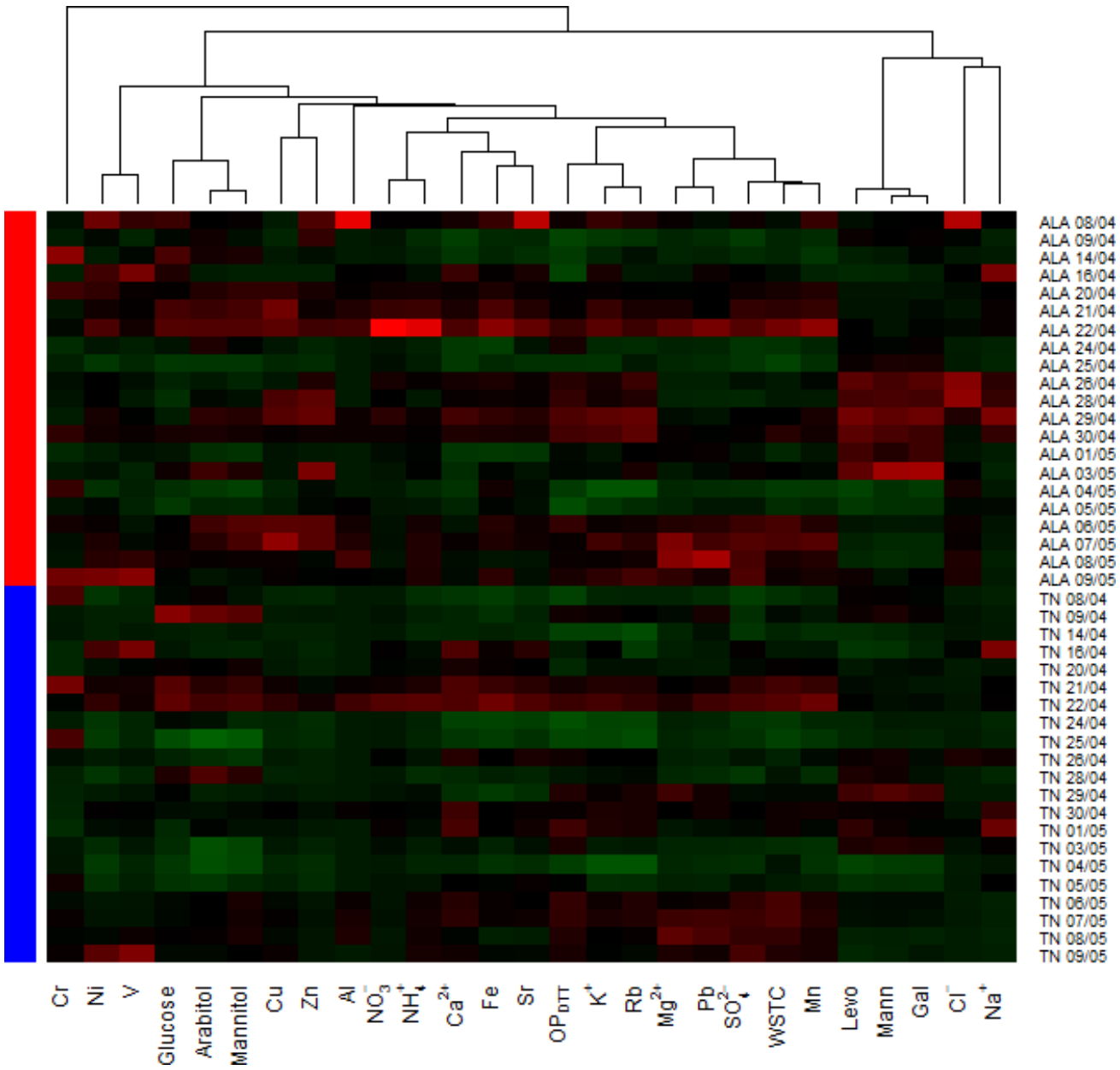
ALA 08/04
ALA 09/04
ALA 14/04
ALA 16/04
ALA 20/04
ALA 21/04
ALA 22/04
ALA 24/04
ALA 25/04
ALA 26/04
ALA 28/04
ALA 29/04
ALA 30/04
ALA 01/05
ALA 03/05
ALA 04/05
ALA 05/05
ALA 06/05
ALA 07/05
ALA 08/05
ALA 09/05
TN 08/04
TN 09/04
TN 14/04
TN 16/04
TN 20/04
TN 21/04
TN 22/04
TN 24/04
TN 25/04
TN 26/04
TN 28/04
TN 29/04
TN 30/04
TN 01/05
TN 03/05
TN 04/05
TN 05/05
TN 06/05
TN 07/05
TN 08/05
TN 09/05
Cr
Ni
V
Glucose
Arabitol
Mannitol
Cu
Zn
Al
NO_3^-
NH_4^+
Ca^{2+}
Fe
Sr
OP_{DTT}
K^+
Rb
Mg^{2+}
Pb
SO_4^{2-}
WSTC
Mn
Levo
Mann
Gal
Cl^-
Na^+

a)

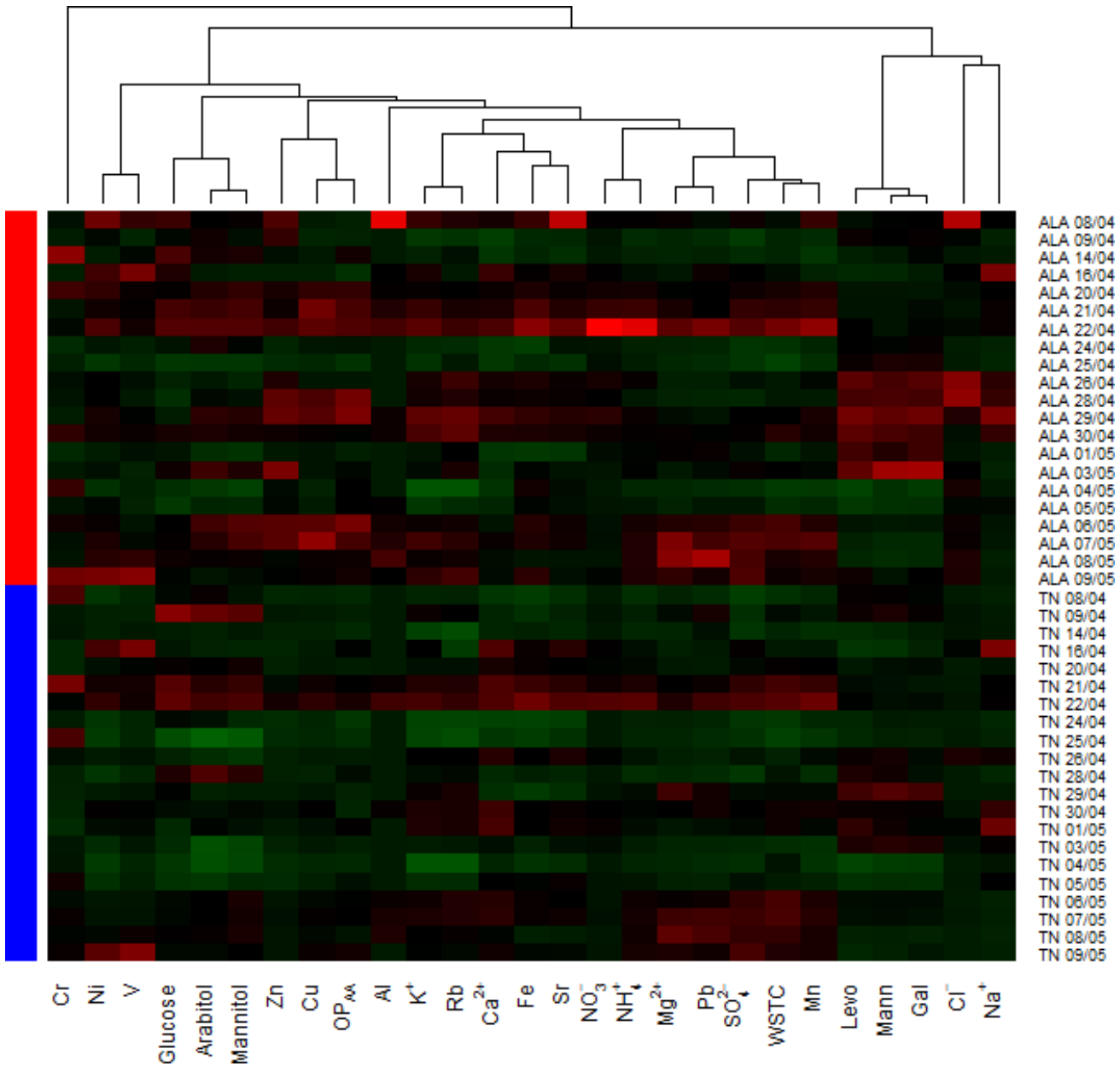
ALA 08/04
ALA 09/04
ALA 14/04
ALA 16/04
ALA 20/04
ALA 21/04
ALA 22/04
ALA 24/04
ALA 25/04
ALA 26/04
ALA 28/04
ALA 29/04
ALA 30/04
ALA 01/05
ALA 03/05
ALA 04/05
ALA 05/05
ALA 06/05
ALA 07/05
ALA 08/05
ALA 09/05
TN 08/04
TN 09/04
TN 14/04
TN 16/04
TN 20/04
TN 21/04
TN 22/04
TN 24/04
TN 25/04
TN 26/04
TN 28/04
TN 29/04
TN 30/04
TN 01/05
TN 03/05
TN 04/05
TN 05/05
TN 06/05
TN 07/05
TN 08/05
TN 09/05
Cr
Ni
V
Glucose
Arabitol
Mannitol
Zn
Cu
OP_{AA}
Al
K^+
Rb
Ca^{2+}
Fe
Sr
NO_3^-
NH_4^+
Mg^{2+}
Pb
SO_4^{2-}
WSTC
Mn
Levo
Mann
Gal
Cl^-
Na^+

b)

Supplementary Material

Click here to download Supplementary Material: Supplementary material_15feb.pdf